Journal of
Synchrotron Radiation

ISSN 0909-0495

Received 18 February 2012
Accepted 24 May 2012

Structure determination of Pt-coated Au dumbbells *via* fluctuation X-ray scattering

Gang Chen,[a] Miguel A. Modestino,[b] Billy K. Poon,[a] André Schirotzek,[c] Stefano Marchesini,[c] Rachel A. Segalman,[b] Alexander Hexemer[c] and Peter H. Zwart[a]*

[a]Physical Bioscience Division, Lawrence Berkeley National Laboratories, Berkeley, CA, USA, [b]Department of Chemical and Biomolecular Engineering, University of California, Berkeley, CA, USA, and [c]Advanced Light Source, Lawrence Berkeley National Laboratories, Berkeley, CA, USA. E-mail: phzwart@lbl.gov

A fluctuation X-ray scattering experiment has been carried out on platinum-coated gold nanoparticles randomly oriented on a substrate. A complete algorithm for determining the electron density of an individual particle from diffraction patterns of many particles randomly oriented about a single axis is demonstrated. This algorithm operates on angular correlations among the measured intensity distributions and recovers the angular correlation functions of a single particle from measured diffraction patterns. Taking advantage of the cylindrical symmetry of the nanoparticles, a cylindrical slice model is proposed to reconstruct the structure of the nanoparticles by fitting the experimental ring angular auto-correlation and small-angle scattering data obtained from many scattering patterns. The physical meaning of the refined structure is discussed in terms of their statistical distributions of the shape and electron density profile.

© 2012 International Union of Crystallography
Printed in Singapore – all rights reserved

Keywords: fXS; SAXS; WAXS.

1. Introduction

The vast majority of macromolecular structures are determined by X-ray crystallography, typically providing structural information at the atomic level (Hendrickson, 2000). The availability of these high-resolution structural models is the foundation for a deeper understanding of fundamental processes in biology, the development of new therapeutic drugs, and novel classes of nano-materials (Matthews, 1976; Blundell & Patel, 2004; Ikkala & Brinke, 2002). Owing to difficulties crystallizing large macromolecular complexes, like membrane proteins or molecular machines, X-ray crystallography is rarely the technique of choice for deriving structural information of such systems. Current techniques, such as electron microscopy, used to study large macromolecular complexes derive structural information of complexes in non-native environments and do not allow for the investigation of time-dependent large-scale structural changes. Techniques like small- and wide-angle X-ray scattering (SAXS/WAXS) allow time-resolved studies but have the drawback that the data contain relatively low information content. A possible route for increasing the information content in solution scattering experiments while following the large-scale structural changes of macromolecular complexes in native-like environments is fluctuation X-ray scattering (fXS), a method proposed by Kam (Kam, 1977; Kam *et al.*, 1981). A fXs experiment is performed by collecting scattering patterns of a dilute sample of scatterers at exposure times below the time required for particles to reorient themselves. It can be shown that a large number of these scattering patterns can be used to estimate the average ring angular auto-correlation (RAC) of the scattering pattern of a single particle (Kam, 1977; Kam *et al.*, 1981; Saldin *et al.*, 2009, 2011). While a model experiment has been successfully carried out on gold nanorods (Saldin *et al.*, 2011), ultimately one would like to apply the fXS technique to study macromolecular structures using X-ray free-electron lasers. The scattering intensity from these systems will be inherently weak owing to the low electron density of organic materials and is worsened by the presence of solvents in most cases. In order to obtain any meaningful structural information from such measurements, care must be taken during data handling such as background subtraction. On the structural reconstruction side, the current method of approaching the problem by solving a hyper-phase problem remains computationally intractable (Saldin *et al.*, 2011). Here, we propose a novel data reduction method that can be generally applied to fXS measurements. This method is particularly useful for handling the non-uniform scattering background. Furthermore, the real-space structure is determined in a straightforward manner by using a reverse Monte Carlo type algorithm operating in real space.

2. Experimental

The fXS measurements were carried out on platinum-coated gold dumbbells randomly oriented on silicon nitride windows.

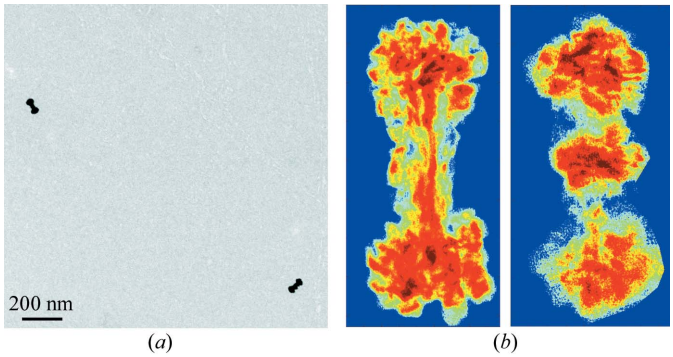

Figure 1
(*a*) TEM image of an enlarged part of the sample under study. (*b*) High-resolution TEM images of two typical nanoparticles used in our study shown in 44 nm by 83 nm rectangular boxes.

The dumbbells were purchased from Sigma-Aldrich in a solution of 100 µg mL^{-1} (http://www.sigmaaldrich.com/, part number 716936). The solution was diluted with deionized water and spin-casted onto the 75 nm-thick silicon nitride substrates. The resulting samples have on average ∼20 dumbbells in a 15 µm-diameter spot as shown in Fig. 1(*a*). Transmission electron microscopy (TEM) measurements with increased resolution were carried out on the samples in the study as shown in Fig. 1(*b*). The X-ray transmission diffraction patterns were collected at beamline 9.0.1 of the Advanced Light Source using highly coherent X-rays with a photon energy of 545 eV. One hundred diffraction patterns were taken from different spots on a single sample, each containing approximately 20 dumbbells. The scattering intensity of each diffraction pattern is normalized by the incident beam intensity recorded before each image was taken.

3. Theoretical considerations

3.1. Experimental data analysis

A typical X-ray transmission diffraction image taken under the above experimental conditions is shown in Fig. 2. As we can see, the scattering from such a diluted system is relatively weak because of the two inherent requirements of a fXS experiment: (i) the scattering interference between different particles must be negligible; (ii) the angular fluctuation must be maintained along rings of equal wavevector transfer in reciprocal space. Both requirements demand having as few particles in the beam as possible, and the net result is a weak scattering intensity. This in turn requires a proper handling of the background scattering. Given the fact that a fluctuation scattering experiment aims to obtain the average ring auto-correlation of the scattering bodies as precisely as possible, it is of vital importance that one corrects for systematic errors in the auto-correlation of the background.

The data reduction method we developed aims to address these issues. The proposed procedure and underlying ideas are not limited to two-dimensional systems and can be used for three-dimensional fXS data analysis as well. We start with converting two-dimensional experimental diffraction data into polar coordinates whose origin coincides with the direct beam position and express all the measured intensities as functions of wave vector transfer, q, and the polar angle, φ. The total scattering intensity, $I_t(q, \varphi)$, can be divided into two parts, one from the nanoparticles [signal, $I_s(q, \varphi)$] and the other accounting for scattering from all other sources such as the substrate and intrinsic background originating from the diffraction set-up [background, $I_b(q, \varphi)$],

$$I_t(q, \varphi) = I_s(q, \varphi) + I_b(q, \varphi). \quad (1)$$

We continue with dividing both the signal and background intensities into two terms, the fluctuation and angularly non-isotropic terms, $I_{sf}(q, \varphi)$ and $I_{bf}(q, \varphi)$, and the mean values along each q, $I_{saxs}(q)$ and $I_{bc}(q)$, so that

$$I_s(q, \varphi) = I_{sf}(q, \varphi) + I_{saxs}(q), \quad (2)$$

$$I_b(q, \varphi) = I_{bf}(q, \varphi) + I_{bc}(q). \quad (3)$$

Substituting them into equation (1), one obtains

$$I_t(q, \varphi) = \left[I_{sf}(q, \varphi) + I_{bf}(q, \varphi)\right] + \left[I_{saxs}(q) + I_{bc}(q)\right]. \quad (4)$$

Subtracting the diffraction pattern by its mean intensity, $I_{saxs}(q) + I_{bc}(q)$, along each diffraction ring, only the fluctuation part of the intensity is left, namely $I_f(q, \varphi)$,

$$I_f(q, \varphi) = I_{sf}(q, \varphi) + I_{bf}(q, \varphi). \quad (5)$$

Because the background intensity comes from sources such as the electronic noise of detectors and unshielded radiation, it is instrument related and does not change during an experiment. For this reason one can assume that the angularly non-isotropic part of the background, $I_{bf}(q, \varphi)$, does not change from image to image. The summation of all the fluctuation terms over all the diffraction images, N, results in

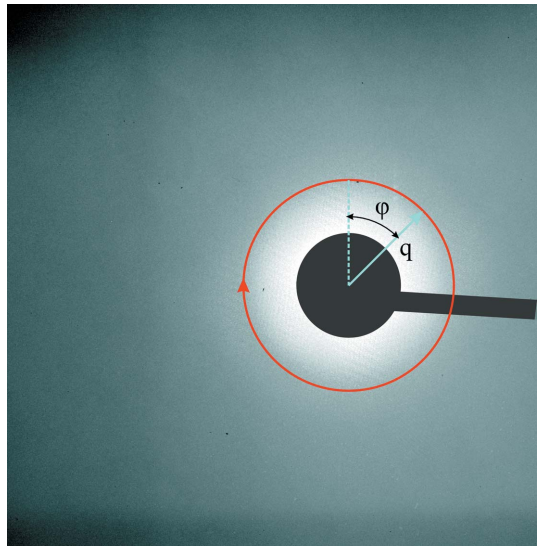

Figure 2
Typical X-ray diffraction pattern of the sample under study.

$$\sum_{n=1}^{N} I_{\rm f}^{n}(q,\varphi) = \sum_{n=1}^{N}\left[I_{\rm sf}^{n}(q,\varphi) + I_{\rm bf}^{n}(q,\varphi)\right] = NI_{\rm bf}(q,\varphi) + \sum_{n=1}^{N} I_{\rm sf}^{n}(q,\varphi). \quad (6)$$

Because the scattering intensity from the particles fluctuates for different diffraction images, the second term in (6) will add up to be zero over a large number of diffraction images (large N),

$$\sum_{n=1}^{N} I_{\rm sf}^{n}(q,\varphi) = 0. \quad (7)$$

From equation (6) we can obtain the fluctuation part of the background scattering,

$$I_{\rm bf}(q,\varphi) = \frac{1}{N}\sum_{n=1}^{N} I_{\rm f}^{n}(q,\varphi). \quad (8)$$

Therefore the fluctuation scattering from the particles can be calculated precisely using the following expression,

$$I_{\rm sf}^{n}(q,\varphi) = I_{\rm f}^{n}(q,\varphi) - \frac{1}{N}\sum_{n=1}^{N} I_{\rm f}^{n}(q,\varphi), \quad (9)$$

where $I_{\rm f}^{n}(q,\varphi)$ can be obtained experimentally as shown in (5). Once the background has been removed, the RAC can be obtained *via*

$$C^{n}(q,\Delta\varphi) = \frac{1}{N_{\varphi}}\sum_{\varphi} I_{\rm sf}^{n}(q,\varphi)\, I_{\rm sf}^{n}(q,\varphi+\Delta\varphi), \quad (10)$$

where N_{φ} is the number of angular divisions along a ring of equal q.

3.2. Structure modeling

In order to recover the real-space structure of the nanoparticles, we applied a reverse Monte Carlo (Metropolis *et al.*, 1953) type method by iteratively comparing the computed and experimental two-dimensional ring auto-correlation data. This method starts with constructing a real-space model and then uses the model to simulate the experimentally measurable data. Here we propose a cylindrically symmetric model for the measured nanoparticles for two reasons: first the particles are cylindrically shaped by growth and second they randomly lie on their sides with the orientation of the particles being uniform along the cylindrical axis. Accordingly, our model simulates the shape of the nanoparticles by many thin discs along its symmetry axis with variable diameters. In this model the scattering amplitude from a cylinder can be calculated analytically using the Born approximation (Als-Nielsen & McMorrow, 2001). Assuming the incident X-ray beam is perpendicular to the cylindrical axis (y-axis), the X-ray scattering amplitude from a cylinder is

$$A(q_r, q_y) = 2\pi\rho r_0 R^2 H\, \frac{J_1(q_r R)}{q_r R}\, \mathrm{sinc}\left[q_y (H/2)\right], \quad (11)$$

where $\mathrm{sinc}(x) = \sin(x)/x$, ρ is the electron density, r_0 is the Thomson scattering length, R and H are the radius and length of the nanorod, respectively, q_r and q_y are the components of wave vector transfer perpendicular and parallel to the cylindrical axis, and J_1 is the Bessel function of the first kind (McAlister & Grady, 1998). To demonstrate how to calculate the X-ray scattering intensities and RAC of a cylindrically symmetric particle by applying equation (11), we take a dumbbell-shaped gold nanoparticle as an example. The total length of this nanoparticle is 80 nm, the radius of the central cylinder is 12.5 nm, and the radius of the balls on both ends is 15 nm. Using the cylindrical slice model, the X-ray scattering pattern of such a nanoparticle can be computed by dividing it into many small slices along its symmetrical axis as shown in Fig. 3(*a*) and each slice can be approximated as a thin disc with its X-ray scattering amplitude calculated by (11). The total scattering intensity from such a particle shown in Fig. 3(*b*) is

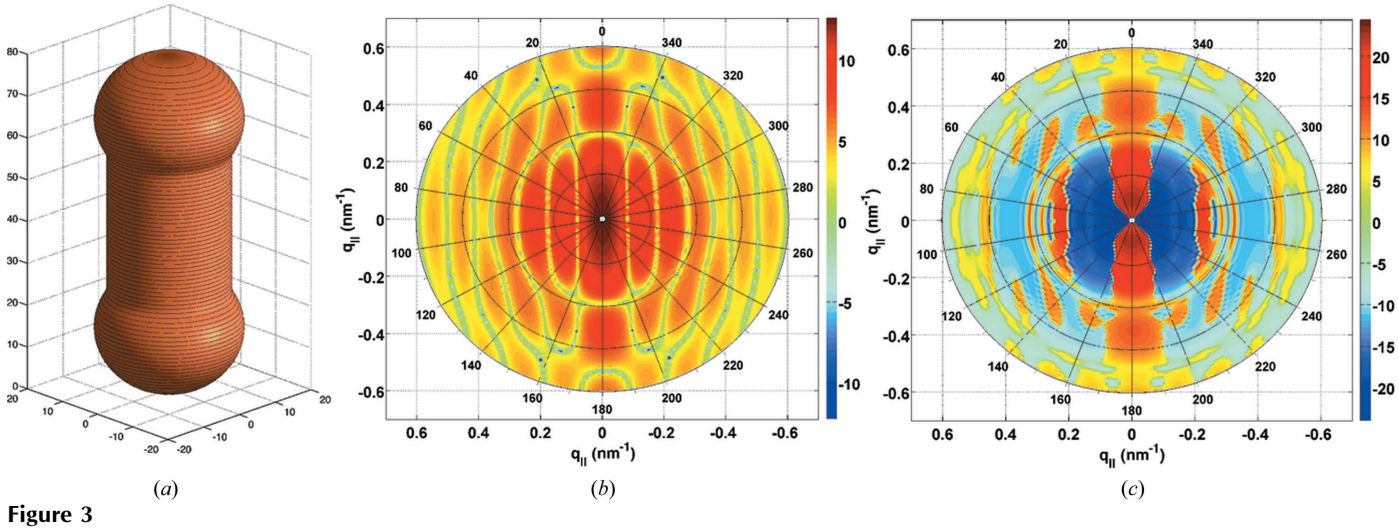

(*a*) (*b*) (*c*)

Figure 3
(*a*) Three-dimensional view of a dumbbell with slices along the symmetry axis representing the cylinders used in the model. The total length of the dumbbell is 80 nm, the radius of the central cylinder is 12.5 nm and the radius for the balls on the two ends is 15 nm. (*b*) X-ray scattering pattern of the dumbbell-shaped gold nanoparticle and (*c*) RAC calculated from its diffraction pattern. (Note, both the X-ray scattering pattern and the RAC are plotted in their natural logarithm values.)

the modulus square of the sum of the scattering amplitude from all the cylindrical slices taking into account the positional phase shift for each slice. Finally, the RAC can be computed from the X-ray scattering pattern which is displayed in Fig. 3(*c*).

4. Results and discussions

The two-dimensional data obtained in the experiment were processed by the outlined data reduction method. Owing to the nature of the experimental set-up, a significant non-uniform scattering background, $I_{\rm bf}(q, \varphi)$, was present in the data as can be seen in Fig. 4(*a*). This scattering background is effectively subtracted from the recorded diffraction pattern following the procedures described in the previous section, and the fluctuation scattering signal, $I^n_{\rm sf}(q, \varphi)$, from the nanoparticles can be obtained for each diffraction pattern. In our sample the nanoparticles are randomly oriented about the incident X-ray beam which is perpendicular to the substrate, and they are so well spread and randomly positioned that the interparticle interference is negligible (Saldin *et al.*, 2010). The resulting X-ray diffraction pattern is a superposition of those of individual nanoparticles, and its RAC, $C^n(q, \Delta\varphi)$, consists of two terms, the single-particle auto-correlation and the interparticle cross-correlation. According to Kam (1977), the average of a large number of $C^n(q, \Delta\varphi)$ will lead to the cancellation of the second term due to the random orientations of the nanoparticles and converge to the RAC of a single nanoparticle, $C^{\rm s}(q, \Delta\varphi)$,

$$C^{\rm s}(q, \Delta\varphi) = \frac{1}{N_{\rm dp}N_{\rm ap}} \sum_n C^n(q, \Delta\varphi), \qquad (12)$$

where $N_{\rm dp}$ is the total number of diffraction patterns collected and $N_{\rm ap}$ is the average number of particles in each diffraction pattern. The RAC shown in Fig. 4(*b*) is a result of averaging 100 RACs calculated using equation (10) (the pattern begins to converge after averaging about 40 RACs).

The structure of the nanoparticles is reconstructed by dividing it into 80 1 nm-high cylindrical slices along its symmetry axis. Owing to the low contrast between Pt and Au, the presence of a coating is not detectable in our experiment and a uniform electron density distribution is considered in our model. Assuming the central symmetry of the nanoparticle, there are only 40 independent radial parameters that we used to optimize the function,

$$\sum_{q,\varphi} \left| C^{\rm exp}(q, \varphi) - C^{\rm calc}(q, \varphi) \right|^2, \qquad (13)$$

where $C^{\rm exp}(q, \varphi)$ and $C^{\rm calc}(q, \varphi)$ are the experimental and calculated RACs. A global optimization algorithm called Covariance Matrix Adaptation Evolution Strategy (CMAES) (Hansen & Ostermeier, 2001) is used to determine optimal model parameters. We start the fitting process with a cylinder of equal radii and the CMAES algorithm iteratively varies their values to minimize the objective function (13). Additional smoothness restraints on the radii of neighbouring cylinders were added to the target function to obtain numerically stable fitting results. Typically, the whole fitting and optimization process completes within a few hours on a desktop computer. The simulated RAC and the three-dimensional view of the structure of the nanoparticles are shown in Fig. 5.

From the TEM measurements shown in Fig. 1(*b*), we note that the nanoparticles in our samples are not exactly the same at the nanometer scale but they all have very similar dimensions in length and diameter. In this case the structure we obtained from fitting to the experimental RAC represents the statistical average of all the nanoparticles in the sample rather than any single one of them. As shown in Fig. 5(*b*), there are seven radial maxima along the symmetry axis, and these are the one at the center and the three at both sides appearing at

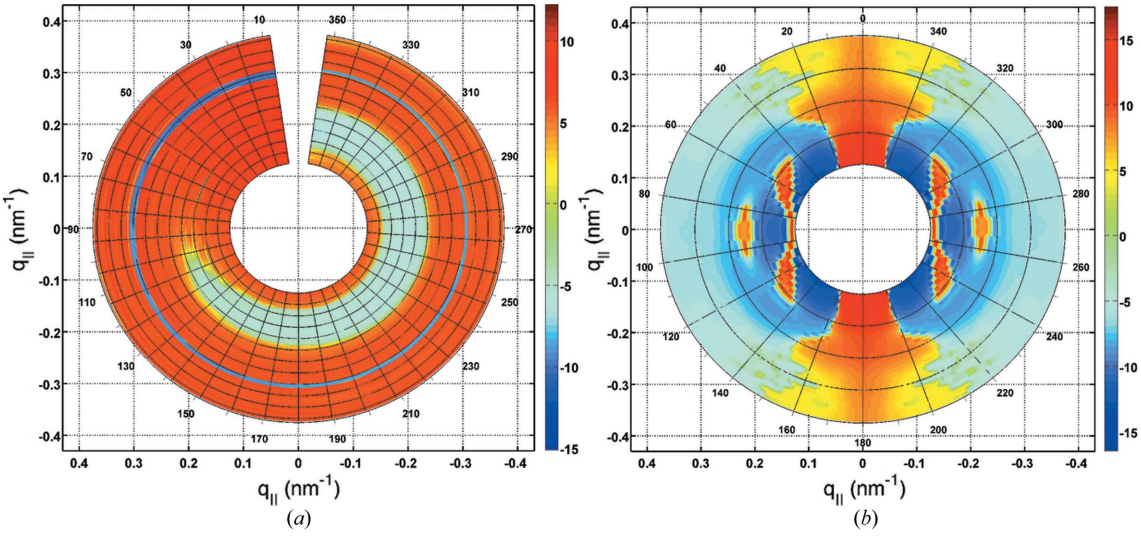

Figure 4
(*a*) Experimental non-uniform scattering background. (*b*) Experimental RAC of a single nanoparticle obtained by averaging RACs of 100 diffraction patterns. (Both figures are plotted in their natural logarithm values.)

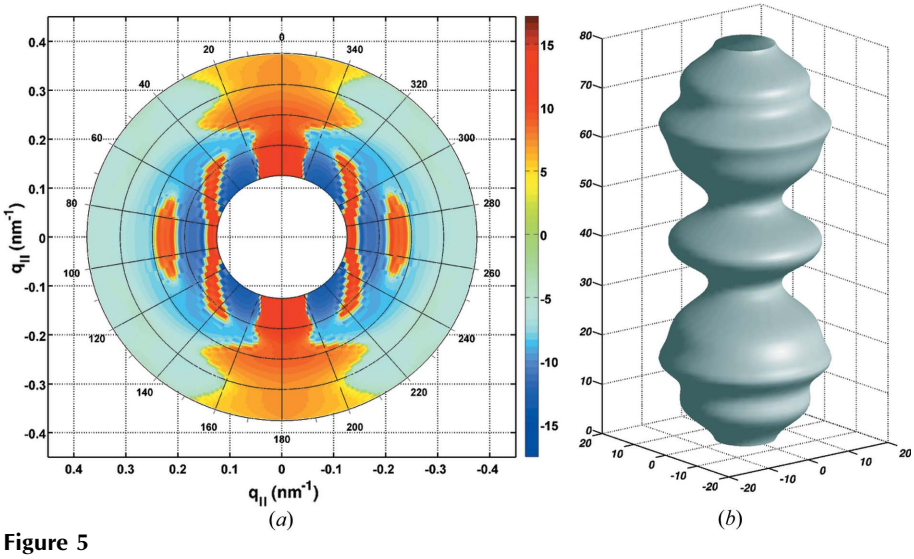

Figure 5
(*a*) Simulated RAC (in natural logarithm values) from a nanoparticle. (*b*) Three-dimensional view of the nanoparticle structure resulting from fitting to the experimental RAC data (all axes are in units of nm).

18 nm, 24 nm and 33 nm away from the center with radii of 15 nm, 14.7 nm, 17 nm and 12.7 nm, respectively. The two apparent minima at 9 nm from the center on both sides have a radius of 7.2 nm. All these features in the structure possibly reflect the general growth preference of the nanoparticles. While the central bulge is not an artifact from structure modeling, it can be caused by multiple effects. Apart from the bulges carried by some particles from growth (more than one-third of 50 particles we measured with TEM have a middle bulge), it could also be caused by standing and incomplete particles as have been observed in the gold nanorod experiment (Saldin *et al.*, 2011). The projection of a standing particle along the X-ray beam has a circular shape and the incomplete parts are mainly the heads of the particles which have circular shapes as well. Both of them will contribute to the middle bulge in the resulting structure along with that coming from growth.

Finally, we note from equation (4) that the small-angle X-ray scattering (SAXS) intensity, $I_{\rm saxs}$, comes concurrently with a fXS experiment. Physical models and computational routines have been developed over the years to extract structural information from experimental SAXS data (Svergun, 1999; Liu *et al.*, 2012). Owing to the nature of our experiment, we do not take into account out-of-plane rotations and the orientational averaging is confined in two dimensions for structure modeling. To be consistent and make the results comparable, we apply the same cylindrical slice model as proposed in the previous section to fit the SAXS data from our experiment. The fitting to the experimental data is very satisfactory as shown in Fig. 6(*a*) with the resulting structural model displayed in Fig. 6(*b*). As we can see from the structures in Fig. 5(*b*) and Fig. 6(*b*), they agree very well in overall profile, with the structure from RAC fitting giving more detail as expected (Kam, 1977). The fact that the nanoparticles in our sample are not monodisperse and microscopically vary in shape and density has different effects on the SAXS and RAC data and hence the structures from their fittings. The full interpretation of the effect involves detailed knowledge of electron density profiles of the nanoparticles obtained from other techniques such as TEM and is currently under way. In a simplified picture, however, the difference comes because the SAXS intensity is always positive while the RAC signal fluctuates around zero and the effect of electron density variation accumulates for the SAXS signal while it can be cancelled for the RAC signal.

5. Conclusions

In conclusion, we have demonstrated the ability of nanoscale structure reconstruction from a random assembly of particles on a substrate using the fluctuation X-ray scattering technique. The structures are determined by reverse Monte Carlo method with a direct fitting to the single-particle RAC and SAXS signals obtained from X-ray diffraction patterns. Even though we have taken advantage of the cylindrical symmetry of the nanoparticles to simplify the fitting process, such a

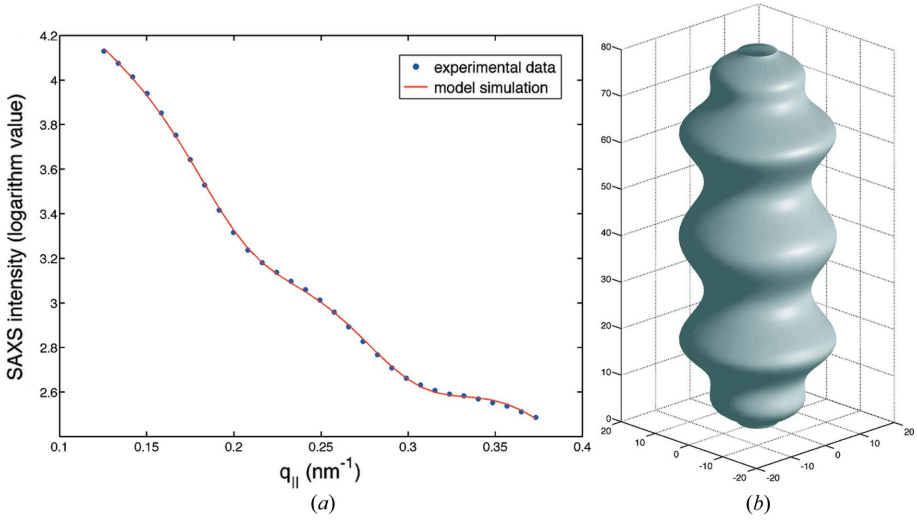

Figure 6
(*a*) Experimental and model simulated small-angle X-ray scattering (SAXS) intensity (in their natural logarithm values) plotted as a function of wave vector transfer. (*b*) Three-dimensional view of the nanoparticle structure resulting from fitting to the experimental SAXS data (all axes are in units of nm).

method can be generalized and used in structure determination *via* fluctuation X-ray scattering with minimal prior knowledge of the structure itself. The results from these simple experiments indicate that a real-space-based approach to determining the structure of a particle in solution is feasible in principle with a further development of real-space modeling techniques and of the associated optimization process. With the help of powerful modern light sources, such as the X-ray free-electron laser, this method is well suited to solving protein structures where the substances are difficult to crystallize. It is not only able to resolve structures in detail comparable with those obtained from protein crystallography, but also provides a way to study them under their native environment in a time-resolved manner.

This work was supported by the Laboratory Directed Research and Development Program of Lawrence Berkeley National Laboratory under US Department of Energy Contract No. DE-AC02-05CH11231.

References

Als-Nielsen, J. & McMorrow, D. (2001). *Elements of Modern X-ray Physics*. New York: Wiley.
Blundell, T. L. & Patel, S. (2004). *Curr. Opin. Pharmacol.* **4**, 490–496.
Hansen, N. & Ostermeier, A. (2001). *Evol. Comput.* **9**, 159–195.
Hendrickson, W. A. (2000). *Trends Biochem. Sci.* **25**, 637–643.
Ikkala, O. & ten Brinke, G. (2002). *Science*, **295**, 2407–2409.
Kam, Z. (1977). *Macromolecules*, **10**, 927–934.
Kam, Z., Koch, M. H. J. & Bordas, J. (1981). *Proc. Natl. Acad. Sci. USA*, **78**, 3559–3562.
Liu, H., Morris, R. J., Hexemer, A., Grandison, S. & Zwart, P. H. (2012). *Acta Cryst.* A**68**, 278–285.
McAlister, B. C. & Grady, B. P. (1998). *J. Appl. Cryst.* **31**, 594–599.
Matthews, B. W. (1976). *Annu. Rev. Phys. Chem.* **27**, 493–523.
Metropolis, N., Rosenbluth, A. W., Rosenbluth, M. N., Teller, A. H. & Teller, E. (1953). *J. Chem. Phys.* **21**, 1087–1092.
Saldin, D. K., Poon, H. C., Bogan, M. J., Marchesini, S., Shapiro, D. A., Kirian, R. A., Weierstall, U. & Spence, J. C. (2011). *Phys. Rev. Lett.* **106**, 115501.
Saldin, D. K., Poon, H. C., Shneerson, V. L., Howells, M., Chapman, H. N., Kirian, R. A., Schmidt, K. E. & Spence, J. C. H. (2010). *Phys. Rev. B*, **81**, 174105.
Saldin, D. K., Shneerson, V. L., Fung, R. & Ourmazd, A. (2009). *J. Phys. Condens. Matter*, **21**, 134014.
Svergun, D. I. (1999). *Biophys. J.* **76**, 2879–2886.